AGU PUBLICATIONS

JGR

Journal of Geophysical Research: Solid Earth

RESEARCH ARTICLE
10.1002/2017JB014201

Key Points:
- Removal of sedimentary reverberations enables reliable determination of crustal thickness and V_p/V_s beneath the Upper Mississippi Embayment
- Receiver function and gravity modeling reveal a mafic high-density upper crust beneath the UME and normal crust beneath Ozark Uplift
- Mafic crustal intrusion occurred in Cretaceous, probably from the passage of a mantle plume, and is responsible for renewed subsidence

Supporting Information:
- Supporting Information S1

Correspondence to:
S. S. Gao,
sgao@mst.edu

Citation:
Liu, L., S. S. Gao, K. H. Liu, and K. Mickus (2017), Receiver function and gravity constraints on crustal structure and vertical movements of the Upper Mississippi Embayment and Ozark Uplift, *J. Geophys. Res. Solid Earth*, *122*, 4572–4583, doi:10.1002/2017JB014201.

Received 12 MAR 2017
Accepted 27 MAY 2017
Accepted article online 1 JUN 2017
Published online 15 JUN 2017

Receiver function and gravity constraints on crustal structure and vertical movements of the Upper Mississippi Embayment and Ozark Uplift

Lin Liu[1], Stephen S. Gao[1], Kelly H. Liu[1], and Kevin Mickus[2]

[1]Geology and Geophysics Program, Missouri University of Science and Technology, Rolla, Missouri, USA, [2]Department of Geography, Geology, and Planning, Missouri State University, Springfield, Missouri, USA

Abstract The Upper Mississippi Embayment (UME), where the seismically active New Madrid Seismic Zone resides, experienced two phases of subsidence commencing in the Late Precambrian and Cretaceous, respectively. To provide new constraints on models proposed for the mechanisms responsible for the subsidence, we computed and stacked *P*-to-*S* receiver functions recorded by 49 USArray and other seismic stations located in the UME and the adjacent Ozark Uplift and modeled Bouguer gravity anomaly data. The inferred thickness, density, and V_p/V_s of the upper and lower crustal layers suggest that the UME is characterized by a mafic and high-density upper crustal layer of ~30 km thickness, which is underlain by a higher-density lower crustal layer of up to ~15 km. Those measurements, in the background of previously published geological observations on the subsidence and uplift history of the UME, are in agreement with the model that the Cretaceous subsidence, which was suggested to be preceded by an approximately 2 km uplift, was the consequence of the passage of a previously proposed thermal plume. The thermoelastic effects of the plume would have induced wide-spread intrusion of mafic mantle material into the weak UME crust fractured by Precambrian rifting and increased its density, resulting in renewed subsidence after the thermal source was removed. In contrast, the Ozark Uplift has crustal density, thickness, and V_p/V_s measurements that are comparable to those observed on cratonic areas, suggesting an overall normal crust without significant modification by the proposed plume, probably owing to the relatively strong and thick lithosphere.

1. Introduction

The Transportable Array (TA) component of the USArray project, which started in 2004 and has recently completed its coverage of the contiguous United States, has produced a broadband seismic data set at stations ~70 km apart with unprecedented quality and spatial coverage, enabling the investigation of a wide spectrum of significant problems related to the structure and processes in the Earth's interior. This study takes advantage of the outstanding data set from the TA and other networks and employs a recently developed modified version of a widely used technique for crustal studies, the H-κ (or thickness-V_p/V_s) stacking [*Zhu and Kanamori*, 2000; *Yu et al.*, 2015a], to delineate crustal thickness and V_p/V_s in the vicinity of the Upper Mississippi Embayment (UME) and the neighboring Ozark Uplift, two of the most significant geological features of the central United States.

1.1. Tectonic Setting

The UME (Figure 1), where the seismically active New Madrid Seismic Zone (NMSZ) resides, is a broad southwest plunging trough with a complex rifting, uplift, and subsidence history in the heart of the relatively stable North American continent [*Mooney et al.*, 1983; *Thomas*, 1991; *Catchings*, 1999; *Van Arsdale and Cox*, 2007]. The center of the UME is occupied by the Reelfoot Rift formed within the Precambrian Eastern Granite-Rhyolite Province (1470 ± 30 Ma) and Southern Granite-Rhyolite Province (1370 ± 30 Ma) [*Van Schmus*, 1992]. The granite provinces are also home to the Ozark Uplift, a 150,000 km^2 intracratonic highland region located to the west of the Reelfoot Rift and eroded to expose Precambrian granites and rhyolites [*Van Schmus*, 1992; *Liang and Langston*, 2009].

Unlike many other continental rifts which have a single phase of subsidence [e.g., *Logatchev and Florensov*, 1978; *Keller et al.*, 1991], the Reelfoot Rift experienced two distinct phases of subsidence separated by about

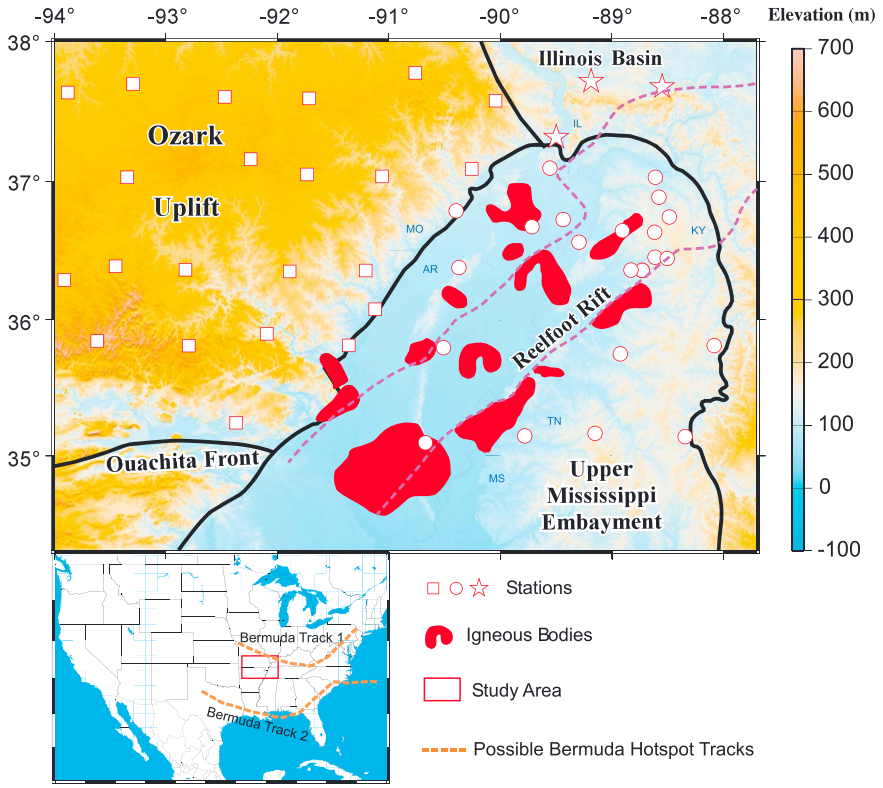

Figure 1. Topographic map showing boundaries of major tectonic features (black lines), igneous bodies (red areas) [*Hildenbrand et al.*, 1996], and broadband seismic stations used in the study. Stations represented by squares, circles, and stars are located in the Ozark Uplift, Upper Mississippi Embayment, and the Illinois Basin, respectively. The area between the purple dashed lines is the Reelfoot Rift, in which the NMSZ is located. The inset in the lower left corner displays the map of the contiguous United States showing the location of study area (red rectangle) and proposed possible Bermuda hotspot tracks (orange dash lines) [*Pollitz and Mooney*, 2014].

250 Ma of relative tectonic quiescence [*Ervin and McGinnis*, 1975]. The initial rifting phase began during the Late Precambrian, when the North American Plate experienced wide-spread rifting events [*Ervin and McGinnis*, 1975]. The major basinal development period was in the Cambrian-Ordovician time, as determined by drilling [*Schwalb*, 1969; *Ervin and McGinnis*, 1975]. The second phase of subsidence, which was responsible for the accumulation of several kilometers of deltaic and marine sediments and was coeval with the emplacement of mafic igneous intrusives found inside and along the shoulders of the rift (Figure 1), started in the Cretaceous and may have continued until the present time and is believed to be the ultimate cause of the high seismicity level in the NMSZ [*Mooney et al.*, 1983; *Hildenbrand and Hendricks*, 1995; *Cox and Van Arsdale*, 2002].

Several models have been proposed for the second (or reactivation) phase of subsidence. The first model attributes the renewed subsidence of the UME to the extensional stress regime associated with the opening of the Gulf of Mexico [*Ervin and McGinnis*, 1975; *Kane et al.*, 1981]. However, this model has been questioned because the subsidence did not start until about 80 Ma after the cessation of the rifting of the Gulf margin [*Cox and Van Arsdale*, 1997]. The second model postulates that the later phase of subsidence of the UME represents isostatic adjustment of a high-density, mafic lower crustal layer during a period of decreased lithospheric viscosity owing to increased geothermal gradient [*DeRito et al.*, 1983; *Braile et al.*, 1986]. The third model advocates the role that the proposed Bermuda mantle plume played during its passage over the previously rifted area [*Cox and Van Arsdale*, 1997], leading to uplift, intrusion of high-density igneous rocks into the crust, erosion of the uplifted axial area of the UME, and subsidence due to thermal contraction and loading of both the sediments and dense intrusions [*Cox and Van Arsdale*, 1997].

This study aims at providing constraints on the proposed subsidence models by measuring crustal thickness and the bulk composition beneath the UME and the adjacent Ozark Uplift. It represents the first joint receiver function (RF) and gravity data investigation of the crustal thickness, V_p/V_s, and density for the study area.

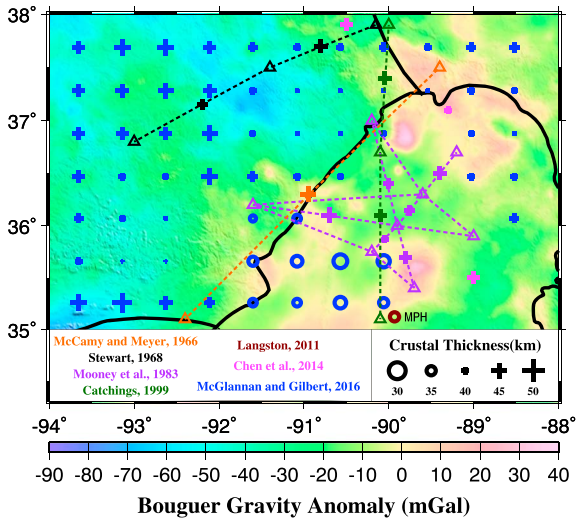

Figure 2. Previous determinations of crustal thickness plotted on top of Bouguer gravity anomalies. Pluses and circles indicate larger and smaller *H* measurements, respectively (see legend). Dashed lines indicate seismic refraction profiles, and triangles are shot points [*McCamy and Meyer*, 1966; *Stewart*, 1968; *Mooney et al.*, 1983; *Catchings*, 1999].

1.2. Previous Crustal Structure Investigations

Numerous geophysical studies have been conducted in the vicinity of the UME over the past decades for the purpose of understanding the formation mechanism of active faults associated with the intracontinental earthquakes occurring in the area. The most significant results regarding crustal thickness, *P* wave velocity, and layered structures were from active-source seismic refraction/wide-angle reflection surveys [*McCamy and Meyer*, 1966; *Mooney et al.*, 1983; *Catchings*, 1999]. One of the major discoveries reported by virtually all the active-source studies is that the lowest 10–20 km of the crust beneath the UME has a V_p of about 7.3–7.4 km/s which is about 10% higher than that of a typical continental lower crust. This lower crustal layer is directly above the Moho, which has a depth of 43–46 km in the UME [*McCamy and Meyer*, 1966; *Mooney et al.*, 1983; *Catchings*, 1999].

Due to the limited spatial coverage of the active-source seismic profiles as a result of the high cost of such experiments, the lateral extent of this layer is not well defined beneath the UME, and the Ozark Uplift was poorly sampled by the above profiles (Figure 2). In addition, because only *P* wave velocities are measured, the V_p/V_s, which is closely related to rock composition and physical properties [*Christensen and Mooney*, 1995], is not available at most of the areas with the exception of a N-S profile of about 400 km length across the UME (Figure 2) [*Catchings*, 1999]. V_p/V_s values were estimated along the profile in several crustal layers, but because the shear wave arrivals cannot be clearly picked, the results suffer from large uncertainties [*Catchings*, 1999].

Source-normalized *P*-to-*S* converted phases from the Moho, i.e., RFs [*Langston*, 1977], have been routinely used to measure crustal thickness (*H*) and most recently V_p/V_s [*Zhu and Kanamori*, 2000] over a large area with relatively low cost. A recent RF study that is most relevant to the present one was conducted by *McGlannan and Gilbert* [2016]. Using RFs recorded by the USArray TA stations, the study concludes that the depth of the Moho beneath the UME is mostly 30–35 km, which is shallower than that of the surrounding areas (40–45 km) and is also shallower than the ~45 km depth reported by most of the active-source seismic studies. Instead of simultaneously searching for both the optimal *H* and V_p/V_s [*Zhu and Kanamori*, 2000], a fixed V_p/V_s of 1.785 was used for the stacking in the *McGlannan and Gilbert* [2016] study, and the results were obtained for overlapping 0.5° by 0.5° bins (rather than at the stations; Figure 2). As demonstrated by the examples shown in Figure 3, RFs in the UME may have been contaminated by strong reverberations generated in the loose sedimentary layer covering most of the UME, and thus, studies using raw RFs might have produced biased results.

1.3. Rationale of the Present Study

Although many previous studies have estimated the crustal thickness beneath the NMSZ and adjacent areas, the active-source seismic experiments were limited to 2-D profiles that traversed only part of the UME (Figure 2) and thus have a limited spatial coverage, making it difficult to compare results from various portions of the UME and with the surrounding areas. More importantly, the calculation of the V_p/V_s, which is crucial for the understanding of tectonic processes that have modified the crust, has yet to be performed on the majority of the stations. The lack of reliable V_p/V_s determinations is most likely caused by the strong reverberations on the RFs associated with the loose sedimentary layer. This study estimates the crustal thickness, V_p/V_s, and density in the UME and adjacent areas through gravity modeling and H-κ stacking after removing the effects of the overlying sediments using a recently developed technique *Yu et al.* [2015a], for the purpose of constraining the subsidence models of the UME.

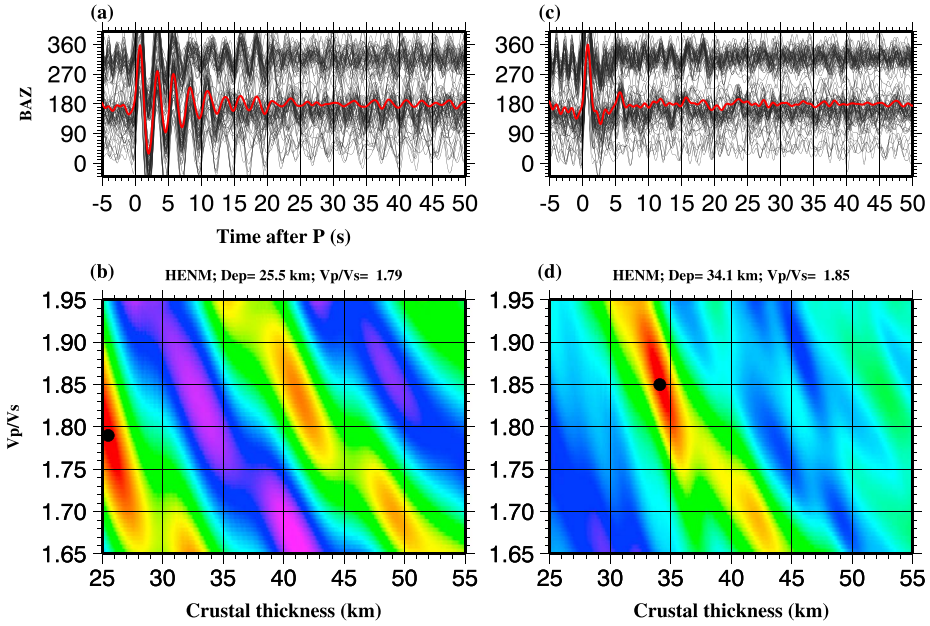

Figure 3. (a) Original RFs from station HENM plotted against back azimuth (BAZ). The red trace is the result of simple time domain summation of the individual RFs and demonstrates the strong decaying periodic arrivals of the reverberations. (b) H-κ stacking using the raw RFs shown in Figure 3a. The dot denotes the maximum stacking amplitude. (c) Same as Figure 3a but for RFs after removing the reverberations using the approach of *Yu et al.* [2015a]. (d) H-κ stacking using the filtered RFs shown in Figure 3c.

2. Data and Methods

All the three-component broadband teleseismic (epicentral distance ≥30°) data were obtained from the Incorporated Research Institutions for Seismology (IRIS) Data Management Center (DMC) within the area of 94°W–88°W and 34°N–38°N (Figure 1) for the time frame from September 1989 to April 2015, when the USArray TA stations completed their recording in the area. A cutoff magnitude (M_c), which is calculated using $M_c = 5.2 + (\Delta - 30.0)/(180.0 - 30.0) - D/700.0$, where Δ and D are the epicentral distance in degree and focal depth in kilometers, respectively, is used to select earthquakes [*Liu and Gao*, 2010].

The seismograms were windowed starting 20 s prior to and extending to 260 s after the first theoretical *P* wave arrival according to the IASP91 Earth model [*Kennett and Engdahl*, 1991]. After being band pass filtered within the frequency range of 0.04 to 1.0 Hz, all the events having a *P* wave signal-to-noise ratio of 4.0 or greater on the radial component were selected and converted into radial RFs using the water level deconvolution procedure described in *Ammon* [1991], with a water level of 0.03 and a Gaussian filter width of 5.0. Subsequently, the radial RFs were inspected visually to keep only the ones with a well-defined first arrival in the 0-2 second window. A total of 7627 high-quality RFs are used in the study.

Strong reverberations in the resulting RFs produced by multiple reflections between the Earth's surface and the bottom of a loose sedimentary layer can seriously mask the *P*-to-*S* converted phases (*PmS*, *PPmS*, and *PSmS*) from the Moho (Figure 3), leading to erroneous crustal thickness and V_p/V_s determinations beneath a recording site [*Zelt and Ellis*, 1999; *Yu et al.*, 2015a]. A resonance-removal filter in the frequency domain is designed to remove or significantly reduce the reverberations [*Yu et al.*, 2015a]. After removing the traveltimes associated with the loose sedimentary layer, the conventional H-κ stacking method [*Zhu and Kanamori*, 2000] can then be employed to determine the crustal thickness and V_p/V_s (Figure 3) beneath the loose sedimentary layer, which is less than 1 km thick in the study area [*Dart and Swolfs*, 1998]. Among the 49 stations that led to reliable H results, 23 were processed with the reverberation removal technique (Table 1). Figure 4 shows examples of the H-κ diagram, and Figures S1–S4 in the supporting information show all the H-κ diagrams and the RFs used to produce them.

An accurate average crustal *P* wave velocity is essential to produce reliable results from the H-κ stacking. Previously estimated average crustal V_p beneath the UME ranges from 6.0 to 6.4 km/s [*Mooney et al.*, 1983;

Table 1. Observations of Crustal Thickness (H, H_n) and V_p/V_s (κ)

Station	Longitude	Latitude	H (km)	κ	H_n (km)	N	Rank
			Ozark Uplift				
HHAR	−93.940	36.282	41.1 ± 0.06	1.800 ± 0.000	–	314	A
LCAR	−91.154	36.070	42.1 ± 0.07	1.790 ± 0.000	–	329	A
MGMO	−92.269	37.154	45.9 ± 0.19	1.823 ± 0.005	–	426	A
S38A	−93.908	37.630	40.6 ± 0.14	1.780 ± 0.009	–	126	A
S39A	−93.323	37.691	44.5 ± 0.14	1.830 ± 0.000	–	221	A
S40A	−92.501	37.599	47.2 ± 0.11	1.754 ± 0.005	–	140	A
S41A	−91.746	37.588	–	–	43.9 ± 0.05	139	B
S42A	−90.794	37.770	42.1 ± 0.34	1.797 ± 0.013	–	99	A
S43A	−90.075	37.572	–	–	41.6 ± 0.06	115	B
T39A	−93.377	37.024	44.2 ± 0.15	1.798 ± 0.004	–	143	A
T41A	−91.764	37.044	43.0 ± 0.19	1.764 ± 0.005	–	115	A
T42A	−91.092	37.030	–	–	39.1± 0.33	151	B
T43A	−90.288	37.083	39.7 ± 0.28	1.771 ± 0.007	–	105	A
U39A	−93.480	36.382	41.1 ± 0.17	1.818 ± 0.004	–	149	A
U40A	−92.854	36.356	39.7 ± 0.15	1.819 ± 0.003	–	333	A
U41A	−91.920	36.344	–	–	44.3 ± 0.23	136	B
U42A	−91.238	36.351	–	–	42.9 ± 0.20	104	B
V39A	−93.645	35.839	–	–	45.2 ± 0.08	151	B
V40A	−92.823	35.804	40.5 ± 0.03	1.800 ± 0.000	–	136	A
V41A	−92.124	35.890	37.6 ± 0.14	1.806 ± 0.005	–	459	A
V42A	−91.390	35.806	38.8 ± 0.16	1.770 ± 0.005	–	101	A
X301[a]	−92.400	35.239	50.3 ± 0.39	1.838 ± 0.004	–	53	A
			Upper Mississippi Embayment				
CUSSO[a]	−89.330	36.552	29.6 ± 0.28	1.879 ± 0.017	–	24	A
DHKY[a]	−88.941	36.635	30.7 ± 0.95	1.869 ± 0.026	–	14	A
HENM[a]	−89.472	36.716	34.0 ± 0.14	1.853 ± 0.007	–	95	A
JLKY[a]	−88.652	36.624	34.4 ± 0.67	1.888 ± 0.028	–	35	A
JRTN[a]	−88.648	36.443	33.3 ± 0.33	1.857 ± 0.013	–	53	A
MMTN[a]	−88.539	36.434	–	–	32.7 ± 0.37	28	B
NKKY[a]	−88.520	36.734	–	–	34.5 ± 0.20	34	B
PARM[a]	−89.752	36.664	37.7 ± 0.22	1.788 ± 0.008	–	104	A
PBMO	−90.430	36.778	40.0 ± 0.14	1.830 ± 0.000	–	545	A
RPTN[a]	−88.763	36.348	32.5 ± 0.35	1.859 ± 0.022	–	29	A
S01[a]	−89.539	36.314	33.6 ± 0.51	1.913 ± 0.016	–	110	A
T44A	−89.590	37.086	–	–	38.6 ± 0.57	103	B
T45A[a]	−88.645	37.020	38.3 ± 0.26	1.867 ± 0.005	–	103	A
U43A[a]	−90.406	36.369	36.0 ± 0.73	1.883 ± 0.016	–	92	A
U45A[a]	−88.763	36.348	32.9 ± 0.24	1.840 ± 0.006	–	40	A
UTMT[a]	−88.864	36.350	31.9 ± 0.27	1.927 ± 0.010	–	263	A
V43A[a]	−90.544	35.786	–	–	26.8 ± 0.16	20	B
V45A[a]	−88.959	35.740	30.4 ± 0.00	1.843 ± 0.005	–	72	A
V46A	−88.118	35.801	–	–	33.9 ± 0.07	76	B
W43A[a]	−90.706	35.088	31.0 ± 0.35	1.864 ± 0.019	–	16	A
W44A[a]	−89.816	35.139	–	–	33.5 ± 0.18	44	B
W45A[a]	−89.186	35.157	–	–	32.7 ± 0.13	124	B
W46A	−88.378	35.133	–	–	37.5 ± 0.23	84	B
WBKY[a]	−88.613	36.877	–	–	37.5 ± 0.09	38	B

Table 1. (continued)

Station	Longitude	Latitude	H (km)	κ	H_n (km)	N	Rank
			Illinois Basin				
FA08	−89.529	37.316	42.0 ± 0.48	1.808 ± 0.018	–	75	A
S44A[a]	−89.217	37.715	44.2 ± 1.11	1.783 ± 0.019	–	1215	A
S45A[a]	−88.580	37.677	–	–	45.9 ± 0.73	146	B

[a] After applying the reverberation removal technique.

Chiu et al., 1992; *Catchings*, 1999; *Ramírez-Guzmán et al.*, 2012]. After considering results from various studies and also the presence of both the low-velocity sedimentary layer and high-velocity lower crust, in this study, we use an average *P* wave velocity of 6.1 km/s, which is the same as that in the IASP91 Earth model. *Nair et al.* [2006] stack 66 CORE (Complete Ordered Ray Expansion) synthetic seismograms to estimate the magnitude of error when an inaccurate V_p is used. They show that if the velocity has a 1% bias, the resulting crustal thickness will be off by about 0.5 km. Likewise, the resulting V_p/V_s will vary by 0.0024 with a 1% bias in V_p. In the study area, previous studies show that the mean crustal velocity is unlikely to depart from 6.1 km/s by more than 5% [*Mooney et al.*, 1983; *Chiu et al.*, 1992; *Catchings*, 1999], corresponding to a possible error of less than 3 km in the resulting H, and less than 0.01 in the V_p/V_s determinations.

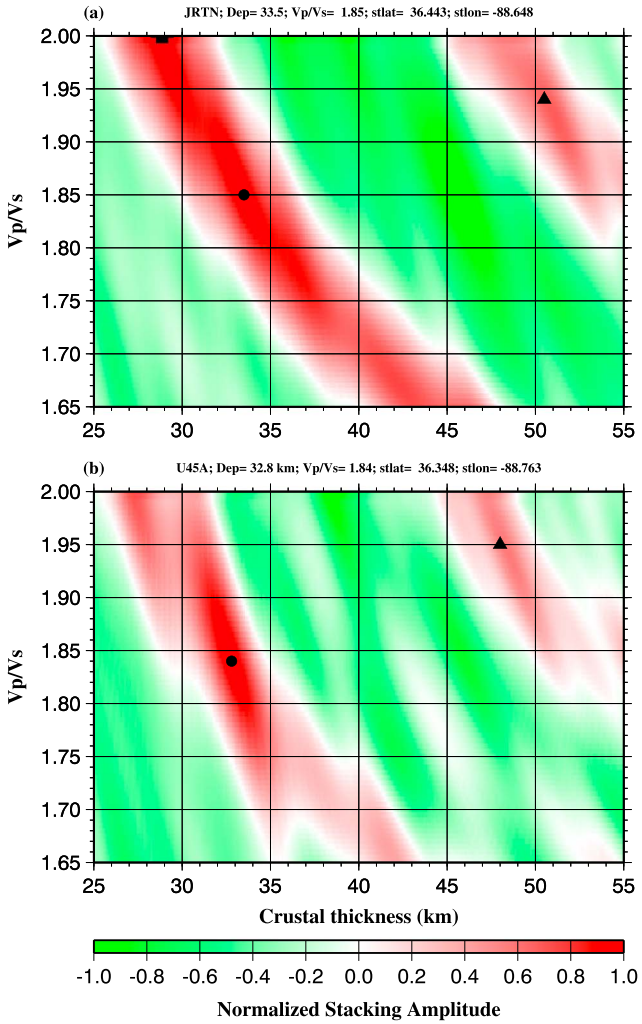

Figure 4. Image of stacking energy from H-κ stacking using the filtered RFs from stations JRTN and U45A located in the UME. The black dots and triangles show points with the first and second largest stacking amplitudes, corresponding to the top and bottom of a lower crustal layer, respectively.

The Bouguer gravity anomaly data consisting of over 69,000 measurement points were obtained from the National Geospatial and Imaging Agency, the United States Geological Survey, and detailed surveys by *Larson and Mickus* [2013] and *Ives et al.* [2014]. The average data spacing of the merged data set ranges from less than 1 km within the UME to 1 – 4 km elsewhere. The merged data set was processed into simple Bouguer gravity anomalies using the 1967 International Gravity formula [*Morelli*, 1976], sea level as a datum, and 2.67 g/cm^3 as a reduction density. Given the lack of significant topographic variations, terrain corrections were not applied.

3. Results

3.1. RF Stacking Results

The 49 stations with observable *PmS* phases on the RFs are divided into categories A and B (Table 1) according to the characteristics of the RFs [*Nair et al.*, 2006]. Stations in category A show a clear *PmS* arrival in the time window of 4 to 8 s, at least one of the *PPmS* and *PSmS* arrivals, and a well-defined peak on the H-κ plot. For category B stations, only the *PmS* is observed, resulting in an ambiguous determination of H and V_p/V_s [*Nair et al.*, 2006]. For these stations, V_p/V_s cannot be reliably determined, and to estimate the crustal thickness, we assume a constant

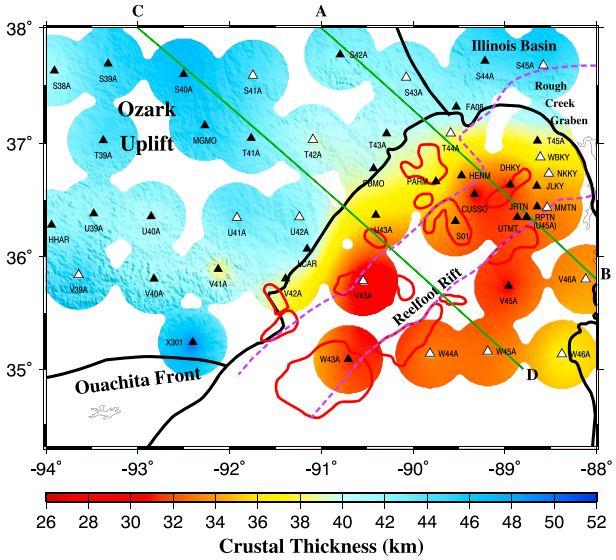

Figure 5. Resulting thickness of the crustal layer corresponding to the maximum stacking amplitude. Filled triangles are category A stations, and open triangles are category B stations. To produce the plot, the observations are fitted using a surface gridding algorithm [*Wessel and Smith*, 1991]. Only areas that are 40 km or closer to a station are shown. Lines A-B and C-D are the locations of the gravity model shown in Figures 7 and 8, respectively.

V_p/V_s based on the average V_p/V_s of category A stations in the same tectonic province (1.85 for stations in the UME and 1.78 for those on the Ozark Uplift) to get the crustal thickness (H_n). Thirty-three stations belong to category A and 16 to category B. In the following discussions, the H measurements for category A and H_n measurements for category B stations are used to qualify crustal thicknesses. Note that due to the influence of the loose sedimentary layer and relatively high noise level suffered by stations on loose sediments, some stations in the UME did not lead to a sufficient number of RFs with clear *PmS* arrivals, even after the reverberation removal technique is applied to the RFs. They are not used in the study.

The observed crustal thicknesses range from 26.8 to 50.3 km with a mean value of 38.4 ± 5.4 km (Figure 5), and the V_p/V_s observations of the 33 category A stations range from 1.75 to 1.93 with an average of 1.83 ± 0.04 (Figure 6). At the stations in the UME, the resulting thickness may not be that of the entire crust; instead, it may be the thickness of the upper crustal layer above a lower crustal layer with anomalously high density and seismic velocity. In other words, it is the vertical distance between the surface and an intracrustal interface. The bottom of the lower crustal layer is hinted in the H-κ plots of some of the stations in the NMSZ (Figure 4) and can also be represented by the deeper arrival shown at most of the stations in the UME (Figures 7 and 8). This weaker interface has a depth of about 45–50 km, which is consistent with crustal thickness from seismic refraction studies [e.g., *Mooney et al.*, 1983; *Catchings*, 1999]. The refraction studies also revealed an intracrustal layer at the depth of 25–30 km beneath the UME [see *Catchings*, 1999, Figures 8 and 9], a value that is comparable to the RF results (Figure 5).

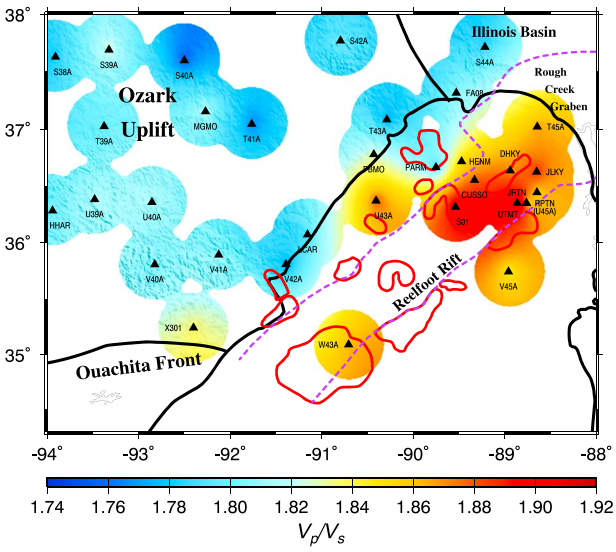

Figure 6. Resulting V_p/V_s measurements obtained at Category A stations.

3.1.1. Ozark Uplift

The crustal thickness measurements obtained using 4045 RFs from 22 stations on the Ozark Uplift range from 37.6 to 50.3 km with a mean value of 42.5 ± 3.0 km, and the V_p/V_s results range from 1.75 to 1.84 with a mean value of 1.80 ± 0.02 (Figures 5 and 6). The crustal thickness values are in general agreement with previous studies for this area [*Chulick and Mooney*, 2002; *Ramírez-Guzmán et al.*, 2012; *Hansen et al.*, 2015; *McGlannan and Gilbert*, 2016]. Both the crustal thickness and V_p/V_s results are typical for the North American cratonic areas [*Keller*, 2013].

3.1.2. UME and Illinois Basin

Almost all the stations in the UME are overlaid with unconsolidated Quaternary sediments, which lead to strong reverberations and a delayed first peak on the RFs (Figure 3a). After reverberation removal and manual checking, 2146 RFs from 24 stations

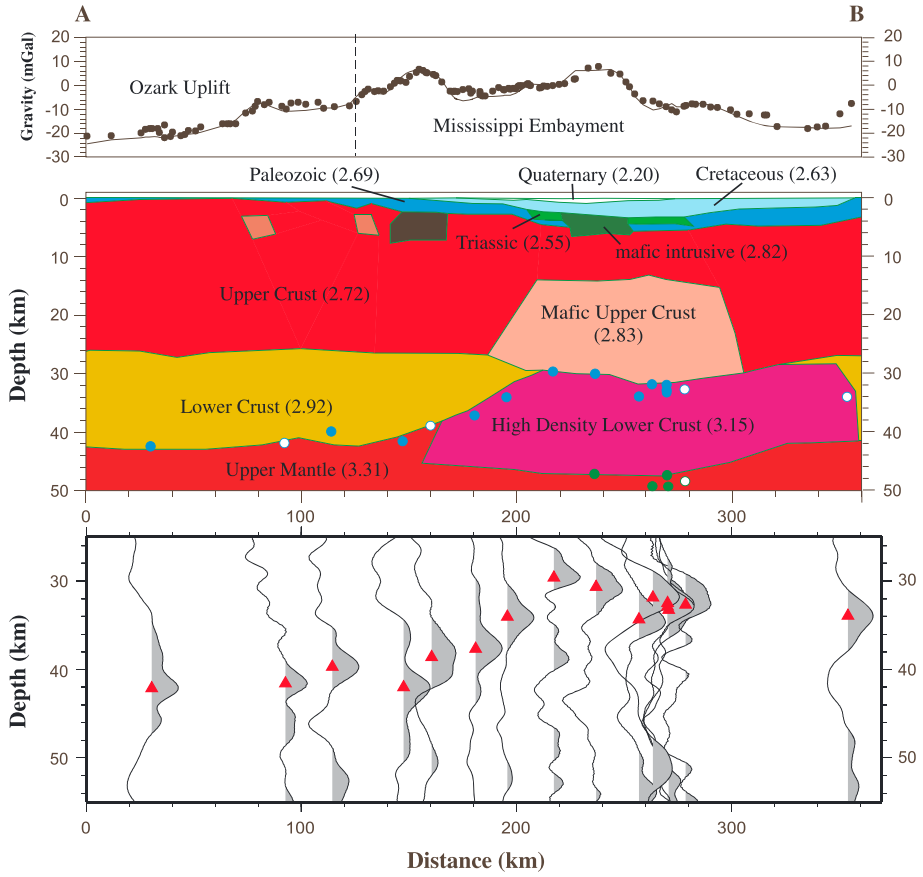

Figure 7. Gravity model of the crust and uppermost mantle and stacked RFs along profile A-B (Figure 5). Densities are in g/cm^3. (top) Observed (black dots) and calculated (solid line) Bouguer gravity anomalies. (middle) Resulting gravity model. Blue circles represent the depth of the arrival on the H-κ plots with the largest stacking amplitude at stations in a 100 km wide band centered on the profile, filled circles are category A stations, open circles are category B stations, and green circles are the approximate depths of the deeper secondary arrival. (bottom) Stacked and depth-converted RFs using the resulting V_p/V_s corresponding to the maximum stacking amplitude on the H-κ plot for each of the stations.

are used for characterizing the crust beneath this area. As discussed earlier, the resulting depth from H-κ stacking represents most likely the top of the high-velocity lower crustal layer, except for a few stations at the edges of the areas. The resulting depths of the interface corresponding to the maximum stacking amplitude on the H-κ plots range from 26.8 to 40.0 km with an average of 33.9 $\pm$ 3.2 km, and the V_p/V_s values are between 1.79 and 1.93 with an average of 1.86 $\pm$ 0.03, suggesting a mafic composition [*Christensen*, 1996]. Another possible cause of the high V_p/V_s is partial melting of crustal rocks [*Watanabe*, 1993]. However, continental areas with pervasive crustal partial melting are usually modern rift zones characterized by high heat flow, greatly thinned crust, negative gravity anomalies, and slower crustal seismic velocities (e.g., *Reed et al.* [2014] for the Afar Depression). These characteristics are generally not associated with the UME.

McGlannan and Gilbert [2016] conducted RF stacking by using a reference V_p of 6.6 km/s [*Catchings*, 1999] and a constant V_p/V_s value of 1.785. The resulting thicknesses corresponding to the largest stacking amplitude are 5–10 km greater than those of ours in this area (Figures 2 and 5). The discrepancy is most likely caused by the different reference *P* wave velocities. Increasing V_p by 8% (from 6.1 to 6.6 km/s) would increase the resulting crustal thickness by nearly 3.7 km. In addition, assuming a V_p/V_s of 1.785 instead of 1.85 can further increase the resulting H by approximately 4 km [*Nair et al.*, 2006].

The southernmost portion of the Illinois Basin is sampled by 1436 RFs recorded at three stations. The observed crustal thicknesses range from 42.0 to 45.9 km, while the V_p/V_s values are from 1.78 to 1.81. The average crustal thickness is 44.0 $\pm$ 1.9 km, and the mean V_p/V_s value is 1.80 $\pm$ 0.02, which is comparable to those observed on the Ozark Uplift but is smaller than those obtained in the UME. The measured crustal thicknesses of *Ramírez-Guzmán et al.* [2012], *Chen et al.* [2014], *Pollitz and Mooney* [2014], and *McGlannan and Gilbert* [2016]

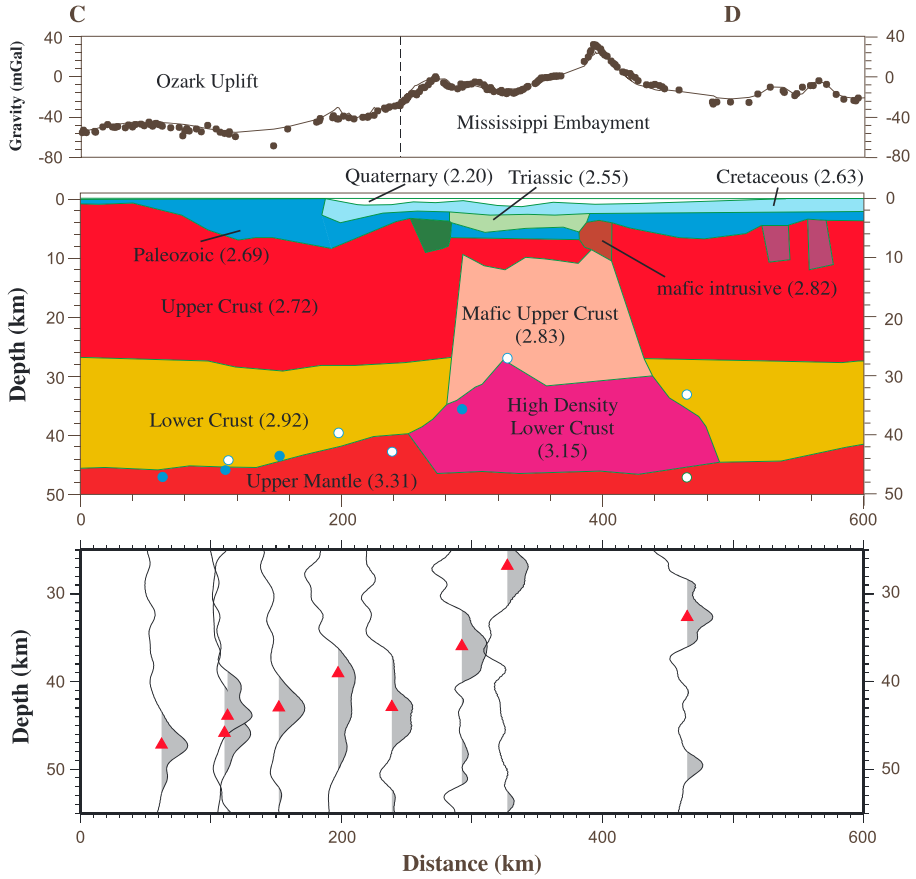

Figure 8. Same as Figure 7 but along profile C-D.

are approximately 40 km beneath the southernmost part of the Illinois Basin, while those of *Hansen et al.* [2015] are greater than 45 km. Therefore, results from this study are in general agreement with those from previous studies.

3.2. Gravity Modeling Results

Modeling of Bouguer gravity anomalies can aid in constraining the crustal structures determined from the seismic results and provide a more detailed image of the upper crustal layer than that determined from broadband seismic modeling [e.g., *Bashir et al.*, 2011; *England and Ebbing*, 2012; *Yu et al.*, 2015b; *Schiffer et al.*, 2016]. Two models along profiles A-B and C-D (Figure 5) were constructed. The forward modeling of the observed Bouguer gravity anomaly data (Figures 7 and 8) was constrained by seismic refraction modeling [*Mooney et al.*, 1983], previous gravity and magnetic analysis [*Hildenbrand*, 1985], and the resulting crustal thickness and V_p/V_s results from the H-κ stacking (Figures 5 and 6) in this study. The H-κ stacking results from this study were used to model the crustal thickness or the thickness of the upper crustal layer beneath the UME. The seismic refraction models [*Mooney et al.*, 1983] were used to constrain the upper crustal geometries, while previous gravity and magnetic studies [*Hildenbrand*, 1985] were applied to estimate the location of the mafic intrusions. The *P* wave velocities from the seismic refraction models of *Mooney et al.* [1983] were converted to densities and used as starting values for the densities in each of the bodies shown in the gravity models. The densities were then varied by a maximum of 15% in order for the calculated gravity values to match the observed gravity anomalies.

The resulting Bouguer gravity anomaly models along profiles A-B and C-D (Figures 7 and 8) are consistent with the existence of both a high-density upper crustal layer and a higher-density lower crustal layer beneath the UME. Like many other continental rifts [*Thybo and Artemieva*, 2013] such as the Baikal [*Thybo and Nielsen*, 2009] and East African rifts [*Birt et al.*, 1997], the Reelfoot Rift is characterized by an upper crustal graben and an altered lower crustal layer [*Mooney et al.*, 1983; *Catchings*, 1999; *Ramírez-Guzmán et al.*, 2012], and the

existence of the high-density upper crustal layer is consistent with the distribution of the relatively high V_p/V_s values (Figure 6).

It is well known that gravity modeling is nonunique. During the modeling process a number of different models were created to determine this nonuniqueness. The gravity modeling alone could not determine the exact thicknesses and densities of the crustal layers nor could it determine if a high-density upper crustal body was required. However, if the high-density upper crustal layer was not modeled, then the crust was thinner (~40 km) than observed under the UME. While this model does roughly fit the available constraints, including the high-density crustal body better explains the high V_p/V_s measurements, and the resulting thicknesses are more consistent with the RF and seismic refraction results.

4. Discussion

4.1. Mafic Intrusion Into the Upper Crustal Layer Beneath the UME

The bulk properties of the crust can be determined by the resulting crustal thickness and V_p/V_s measurements. It is commonly accepted that felsic, intermediate, and mafic rocks have typical V_p/V_s values of smaller than 1.78, between 1.78 and 1.81, and greater than 1.81, respectively [*Christensen*, 1996]. The laboratory measurements made by *Christensen* [1996] also concluded that the average V_p/V_s is approximately 1.74 and 1.81 in the upper and lower crust, respectively, with an average value of 1.78 for the entire continental crust.

The UME is located within the granite-rhyolite provinces [*Van Schmus*, 1992], where the crust was pervasively modified by granitic and associated anorthitic intrusions during the Proterozoic [*Whitmeyer and Karlstrom*, 2007]. As granite is a felsic rock and has a low V_p/V_s value of 1.71, the high V_p/V_s observed beneath the UME most likely reflects intrusion of mafic material into the upper crust. We argue that the mafic intrusion took place during the Cretaceous time, mostly because of the fact that the vast majority of mafic intrusions found near the surface are Cretaceous in age [*Hildenbrand and Hendricks*, 1995], and thus, it is reasonable to assume that mafic intrusions of the same age also exist deep in the crust.

One of the new findings from this study is the likely existence of a mafic high-density upper crustal layer beneath the UME sampled by the broadband seismic stations (Figure 6). Unlike the mafic lower crustal layer which has been identified beneath almost all continental rifts [*Mooney et al.*, 1983; *Keller et al.*, 2006; *Thybo and Nielsen*, 2009; *Birt et al.*, 1997], the existence of a mafic upper crustal layer is rare, if not previously unrecognized, for continental rifts, and might be responsible for the second phase of subsidence the studied UME area has experienced since the Cretaceous through isostatic adjustment.

4.2. Constraints on Subsidence Models

Among the proposed mechanisms for the second phase of subsidence of the UME, including far-field regional extensional stress [*Ervin and McGinnis*, 1975; *Kane et al.*, 1981], episodic variations in lithospheric viscosity due to increased geothermal gradient [*DeRito et al.*, 1983; *Braile et al.*, 1986], and the thermal-elastic effects of a passing mantle plume [*Van Arsdale and Cox*, 2007], the passage of the proposed Bermuda mantle plume is arguably most capable of inducing pervasive igneous intrusions into both the upper and lower crustal layers along previous fractured zones of weakness produced by the initial rifting in the Late Precambrian. This model can also explain the ~2 km uplift of the UME during the Cretaceous [*Van Arsdale and Cox*, 2007; *Hildenbrand et al.*, 1996; *Cox and Van Arsdale*, 2002]. The model further suggests that the plume heated the continental lithosphere, causing it to expand and rise to form an arch which was then eroded to low relief. When the area moved off of the plume, the heavier-than-normal UME crust cooled and sank starting from the Late Cretaceous. The surface was lowered below sea level, resulting in a depression that allowed water from the Gulf of Mexico to invade the area [*Van Arsdale and Cox*, 2007].

It should be pointed out that while our observations are in agreement with the predictions of a passing plume model, the existence of such a plume during the Mesozoic beneath our study area was solely based on conclusions from some of the previous studies. Similar to most other perceived mantle plumes, the origin of the igneous rocks in the UME remains enigmatic, and seismological observations regarding whether the recent Bermuda volcanism is associated with a lower mantle plume, a plume originated in the mantle transition zone, or edge-driven small-scale convection is a debated topic, which requires additional interdisciplinary studies to possibly resolve [*Benoit et al.*, 2013; *Gao and Liu*, 2014].

4.3. Effect of the Possible Thermal Upwelling on the Ozark Uplift

In comparison with the spatial variation of crustal thickness and V_p/V_s measurements in the central U.S. [*Chulick and Mooney*, 2002; *Keller*, 2013], especially the midcontinental cratonic region to the north of the

study area, our observations (42.5 ± 3.0 km and 1.80 ± 0.02) beneath the Ozark Uplift are normal values. Corresponding to the negative Bouguer gravity anomalies and felsic upper crustal layer in our gravity modeling (Figures 7 and 8), a low-density granitic upper crustal layer is implied and can be explained as being derived from the Proterozoic granite-rhyolite intrusion event [*Hildenbrand et al.*, 1996]. Although mafic intrusions occurred beneath the UME, it is apparent that the thermal upwelling could not penetrate the strong cratonic lithosphere of the Ozark Uplift [*Cox and Van Arsdale*, 2002]. The difference in the influence of the passing plume might suggest that the plume could only significantly affect areas of weakness of the continental lithosphere, and the strong cratonic lithosphere can prevent major intrusion, so the crust is essentially unmodified by the passing plume.

5. Conclusions

Observations of crustal properties measured using RFs and gravity anomaly data confirm the existence of a mafic, high-density lower crustal layer beneath the UME, and reveal a high-density mafic upper crustal layer which is not commonly found beneath other continental rifts. The previously inferred dominantly Cretaceous age of the mafic intrusions found in the UME and the approximately 2 km rise of the area preceding the post-Cretaceous subsidence suggest a possible role of a passing mantle plume on the tectonic evolution of the UME. Intrusion of mantle material into the UME crust fractured by rifting during the Late Precambrian increased the bulk density of the crust, leading to renewed subsidence after the plume moved away from the area. The Ozark Uplift, in contrast, is characterized by normal crustal thickness and V_p/V_s measurements that are similar to those of midcontinent cratonic crust, suggesting that the plume did not penetrate the strong and thick lithosphere beneath the Ozark Uplift.

Acknowledgments
Data used in the study were obtained from the IRIS DMC (last accessed: April 2015) and from the National Geospatial and Imaging Agency (last accessed: October 2016). Constructive comments by two anonymous reviewers significantly improved the manuscript. This study was supported by the American Chemical Society Petroleum Research Fund under grant PRF 50903-ND8.

References

Ammon, C. J. (1991), The isolation of receiver effects from teleseismic *P* waveforms, *Bull. Seismol. Soc. Am.*, *81*, 2504–2510.
Bashir, L., S. S. Gao, K. H. Liu, and K. Mickus (2011), Crustal structure and evolution beneath the Colorado Plateau and the southern Basin and Range Province: Results from receiver function and gravity studies, *Geochem. Geophys. Geosyst.*, *12*, 1525–2027, doi:10.1029/2011GC003563.
Benoit, M. H., M. D. Long, and S. D. King (2013), Anomalously thin transition zone and apparently isotropic upper mantle beneath Bermuda: Evidence for upwelling, *Geochem. Geophys. Geosyst.*, *14*, 4282–4291, doi:10.1002/ggge.20277.
Birt, C. S., P. K. H. Maguire, M. A. Khan, H. Thybo, G. R. Keller, and J. Patel (1997), The influence of pre-existing structures on the evolution of the southern Kenya Rift valley: Evidence from seismic and gravity studies, *Tectonophysics*, *278*, 211–242.
Braile, L. W., W. J. Hinze, G. R. Keller, E. G. Lidiak, and J. L. Sexton (1986), Tectonic development of the New Madrid rift complex, Mississippi embayment, North America, *Tectonophysics*, *131*, 1–21, doi:10.1016/0040-1951(86)90265-9.
Catchings, R. D. (1999), Regional V_p, V_s, V_p/V_s, and Poisson's ratios across earthquake source zones from Memphis, Tennessee, to St. Louis, Missouri, *Bull. Seismol. Soc. Am.*, *89*, 1591–1605.
Chen, C., D. Zhao, and S. Wu (2014), Crust and upper mantle structure of the New Madrid Seismic Zone: Insight into intraplate earthquakes, *Phys. Earth Planet. Inter.*, *230*, 1–14, doi:10.1016/j.pepi.2014.01.016.
Chiu, J. M., A. C. Johnston, and Y. T. Yang (1992), Imaging the active faults of the central New Madrid seismic zone using PANDA array data, *Seismol. Res. Lett.*, *63*, 375–393, doi:10.1785/gssrl.63.3.375.
Christensen, N. I. (1996), Poisson's ratio and crustal seismology, *J. Geophys. Res.*, *101*, 3139–3156, doi:10.1029/95JB03446.
Christensen, N. I., and W. D. Mooney (1995), Seismic velocity structure and composition of the continental crust: A global view, *J. Geophys. Res.*, *100*, 9761–9788, doi:10.1029/95JB00259.
Chulick, G. S., and W. D. Mooney (2002), Seismic structure of the crust and uppermost mantle of North America and adjacent oceanic basins: A synthesis, *Bull. Seismol. Soc. Am.*, *92*, 2478–2492, doi:10.1785/0120010188.
Cox, R. T., and R. B. Van Arsdale (1997), Hotspot origin of the Mississippi embayment and its possible impact on contemporary seismicity, *Eng. Geol.*, *46*, 201–216, doi:10.1016/S0013-7952(97)00003-3.
Cox, R. T., and R. B. Van Arsdale (2002), The Mississippi Embayment, North America: A first order continental structure generated by the Cretaceous superplume mantle event, *J. Geodyn.*, *34*, 163–176, doi:10.1016/S0264-3707(02)00019-4.
Dart, R. L., and H. S. Swolfs (1998), Contour mapping of relic structures in the Precambrian basement of the Reelfoot rift, North American midcontinent, *Tectonics*, *17*, 235–249.
DeRito, R. F., F. A. Cozzarelli, and D. S. Hodge (1983), Mechanism of subsidence of ancient cratonic rift basins, *Tectonophysics*, *94*, 141–168, doi:10.1016/0040-1951(83)90014-8.
England, R. W., and J. Ebbing (2012), Crustal structure of central Norway and Sweden from integrated modelling of teleseismic receiver functions and the gravity anomaly, *Geophys. J. Int.*, *191*, 1–11, doi:10.1111/j.1365-246X.2012.05607.x.
Ervin, C. P., and L. D. McGinnis (1975), Reelfoot rift: Reactivated precursor to the Mississippi embayment, *Geol. Soc. Am. Bull.*, *86*, 1287–1295, doi:10.1130/0016-7606(1975)86<1287:RRRPTT>2.0.CO;2.
Gao, S. S., and K. H. Liu (2014), Mantle transition zone discontinuities beneath the contiguous United States, *J. Geophys. Res. Solid Earth*, *119*, 6452–6468, doi:10.1002/2014JB011253.
Hansen, S. M., K. Dueker, and B. Schmandt (2015), Thermal classification of lithospheric discontinuities beneath USArray, *Earth Planet. Sci. Lett.*, *431*, 36–47, doi:10.1016/j.epsl.2015.09.009.
Hildenbrand, T. G. (1985), Rift structure of the northern Mississippi embayment from the analysis of gravity and magnetic data, *J. Geophys. Res.*, *90*, 12,607–12,622, doi:10.1029/JB090iB14p12607.
Hildenbrand, T. G., and J. D. Hendricks (1995), Geophysical setting of the Reelfoot rift and relations between rift structures and the New Madrid seismic zone, US Geol. Surv. E1538, U.S. Geol. Surv., Washington, D. C.

Hildenbrand, T. G., A. Griscom, W. R. Van Schmus, and W. D. Stuart (1996), Quantitative investigations of the Missouri gravity low: A possible expression of a large, Late Precambrian batholith intersecting the New Madrid seismic zone, *J. Geophys. Res.*, *101*, 21,921–21,942, doi:10.1029/96JB01908.

Ives, B., K. Mickus, A. McCafferty, C. Seeger, and M. Starkey (2014), Analyzing the Paleozoic basement structure and lithologies of the northwest St. Francois Terrance, Missouri using gravity data to investigate possible mineral deposits of economic interest, *Geol. Soc. Am. Abstr. Programs*, *46*, 308.

Kane, M. F., T. G. Hildenbrand, and J. D. Hendricks (1981), Model for the tectonic evolution of the Mississippi Embayment and its contemporary seismicity, *Geology*, *9*, 563–568, doi:10.1130/0091-7613(1981).9<563:MFTTEO>.2.0.CO;2.

Keller, G. R. (2013), The Moho of North America: A brief review focused on recent studies, *Tectonophysics*, *609*, 45–55, doi:10.1016/j.tecto.2013.07.031.

Keller, G. R., M. A. Khan, P. Morgan, R. F. Wendlandt, W. S. Baldridge, K. H. Olsen, C. Prodehl, and L. W. Braile (1991), A comparative study of the Rio Grande and Kenya rifts, *Tectonophysics*, *197*, 355–371.

Keller, G. R., R. F. Wendlandt, and M. H. P. Bott (2006), West and central African rift system, *Dev. Geotectonics*, *25*, 437–449.

Kennett, B. L. N., and E. R. Engdahl (1991), Traveltimes for global earthquake location and phase identification, *Geophys. J. Int.*, *105*, 429–465.

Langston, C. A. (1977), The effect of planar dipping structure on source and receiver responses for constant ray parameter, *Bull. Seismol. Soc. Am.*, *67*, 1029–1050.

Larson, M., and K. Mickus (2013), Gravity and magnetic analysis of plutons, ring plutons and mafic bodies in the St. Francois Mountains, SE Missouri, *Geol. Soc. Am. Abstr. Programs*, *45*, 2.

Liang, C., and C. A. Langston (2009), Three-dimensional crustal structure of eastern North America extracted from ambient noise, *J. Geophys. Res.*, *114*, B03310, doi:10.1029/2008JB005919.

Liu, K. H., and S. S. Gao (2010), Spatial variations of crustal characteristics beneath the Hoggar swell, Algeria, revealed by systematic analyses of receiver functions from a single seismic station, *Geochem. Geophys. Geosyst.*, *11*, Q08011, doi:10.1029/2010GC003091.

Logatchev, N. A., and N. A. Florensov (1978), The Baikal system of rift valleys, *Tectonophysics*, *45*, 1–13.

McCamy, K., and R. P. Meyer (1966), Crustal results of fixed multiple shots in the Mississippi embayment, in *The Earth Beneath the Continents*, edited by J. S. Steinhart and T. J. Smith, pp. 370–381, AGU, Washington, D. C., doi:10.1029/GM010p0370.

McGlannan, A. J., and H. Gilbert (2016), Crustal signatures of the tectonic development of the North American midcontinent, *Phys. Earth Planet. Inter.*, *433*, 339–349, doi:10.1016/j.epsl.2015.10.048.

Mooney, W. D., M. C. Andrews, A. Ginzburg, D. A. Peters, and R. M. Hamilton (1983), Crustal structure of the northern Mississippi embayment and a comparison with other continental rift zones, *Tectonophysics*, *94*, 327–348, doi:10.1016/0040-1951(83)90023-9.

Morelli, C. (1976), Modern standards for gravity surveys, *Geophysics*, *41*, 1051, doi:10.1190/1.1440661.

Nair, S. K., S. S. Gao, K. H. Liu, and P. G. Silver (2006), Southern African crustal evolution and composition: Constraints from receiver function studies, *J. Geophys. Res.*, *111*, B02304, doi:10.1029/2005JB003802.

Pollitz, F. F., and W. D. Mooney (2014), Seismic structure of the central US crust and shallow upper mantle: Uniqueness of the Reelfoot Rift, *Earth Planet. Sci. Lett.*, *402*, 157–166, doi:10.1016/j.epsl.2013.05.042.

Ramírez-Guzmán, L., O. S. Boyd, S. Hartzell, and R. A. Williams (2012), Seismic velocity model of the central United States (version 1): Description and simulation of the 18 April 2008 Mt. Carmel, Illinois, earthquake, *Bull. Seismol. Soc. Am.*, *102*, 2622–2645, doi:10.1785/0120110303.

Reed, C. A., S. Almadani, S. S. Gao, A. A. Elsheikh, S. Cherie, M. G. Abdelsalam, A. K. Thurmond, and K. H. Liu (2014), Receiver function constraints on crustal seismic velocities and partial melting beneath the Red Sea rift and adjacent regions, Afar Depression, *J. Geophys. Res. Solid Earth*, *119*, 2138–2152, doi:10.1002/2013JB010719.

Schiffer, C., N. Balling, J. Ebbing, B. H. Jacobsen, and S. B. Nielsen (2016), Geophysical-petrological modelling of the East Greenland Caledonides—Isostatic support from crust and upper mantle, *Tectonophysics*, *692*, 44–57, doi:10.1016/j.tecto.2016.06.023.

Schwalb, H. R. (1969), Paleozoic geology of the Jackson Purchase region, *Kentucky: Kentucky Geol. Surv. Rep. of Invest.*, *10*, 40.

Stewart, S. W. (1968), Crustal structure in Missouri by seismic-refraction methods, *Bull. Seismol. Soc. Am.*, *58*, 291–323.

Thomas, W. A. (1991), The Appalachian-Ouachita rifted margin of southeastern North America, *Geol. Soc. Am. Bull.*, *103*, 415–431, doi:10.1130/0016-7606(1991)103<0415:TAORMO>2.3.CO;2.

Thybo, H., and I. M. Artemieva (2013), Moho and magmatic underplating in continental lithosphere, *Tectonophysics*, *609*, 605–619.

Thybo, H., and C. A. Nielsen (2009), Magma-compensated crustal thinning in continental rift zones, *Nature*, *457*, 873–876, doi:10.1038/nature07688.

Van Arsdale, R. B., and R. T. Cox (2007), The Mississippi's curious origins, *Sci. Am.*, *296*, 76–82.

Van Schmus, W. R. (1992), Tectonic setting of the midcontinent rift system, *Tectonophysics*, *213*, 1–15, doi:10.1016/0040-1951(92)90247-4.

Watanabe, T. (1993), Effects of water and melt on seismic velocities and their application to characterization of seismic reflectors, *Geophys. Res. Lett.*, *20*, 2933–2936.

Wessel, P., and W. H. Smith (1991), Free software helps map and display data, *Eos Trans. AGU*, *72*, 441–446.

Whitmeyer, S. J., and K. E. Karlstrom (2007), Tectonic model for the Proterozoic growth of North America, *Geosphere*, *3*, 220–259, doi:10.1130/GES00055.1.

Yu, Y., J. Song, K. H. Liu, and S. S. Gao (2015a), Determining crustal structure beneath seismic stations overlying a low-velocity sedimentary layer using receiver functions, *J. Geophys. Res. Solid Earth*, *120*, 3208–3218, doi:10.1002/2014JB011610.

Yu, Y., K. H. Liu, C. A. Reed, M. Moidaki, K. Mickus, E. A. Atekwana, and S. S. Gao (2015b), A joint receiver function and gravity study of crustal structure beneath the incipient Okavango Rift, Botswana, *Geophys. Res. Lett.*, *42*, 8398–8405, doi:10.1002/2015GL065811.

Zelt, B. C., and R. M. Ellis (1999), Receiver-function studies in the Trans-Hudson orogen, Saskatchewan, *Can. J. Earth Sci.*, *36*, 585–603, doi:10.1139/cjes-36-4-585.

Zhu, L., and H. Kanamori (2000), Moho depth variation in southern California from teleseismic receiver functions, *J. Geophys. Res.*, *105*, 2969–2980, doi:10.1029/1999JB900322.